Preprint: Bridgelall, R., Bhardwaj B., Lu, P., Tolliver, D., and Dhingra, N. (2022). Detecting Sources of Ride Roughness by Ensemble Connected Vehicle Signals. *International Journal of Pavement Engineering*, DOI: 10.1080/10298436.2022.2069243.

Detecting Sources of Ride Roughness by Ensemble Connected Vehicle Signals

Raj Bridgelall, Ph.D.*
Assistant Professor and Program Director
Department of Transportation, Logistics and Finance, North Dakota State University
NDSU Department 2880 P.O. Box 6050, Fargo, ND 58101-6050
Phone: (408) 607-3214; Email: raj@bridgelall.com; ORCiD: 0000-0003-3743-6652

Bhavana Bhardwaj
Research Assistant
Department of Computer Science, North Dakota State University
NDSU Department 2880 P.O. Box 6050 Fargo, ND 58108-6050,
Phone: (701) 729-1647; Email: bhavana.bhardwaj@ndsu.edu; ORCiD: 0000-0002-4379-1565

Pan Lu, Ph.D.
Associate Professor and Associate Research Fellow
Department of Transportation, Logistics and Finance, North Dakota State University
NDSU Department 2880 P.O. Box 6050, Fargo, ND 58101-6050
Phone: (720) 238-0080; Email: pan.lu@ndsu.edu; ORCiD: 0000-0002-1640-3598

Denver D. Tolliver, Ph.D.
Director
Upper Great Plains Transportation Institute, North Dakota State University
NDSU Department 2880 P.O. Box 6050, Fargo, ND 58108
Phone: (701) 231-7190; Email: denver.tolliver@ndsu.edu; ORCiD: 0000-0002-8522-9394

Neeraj Dhingra
Research Assistant
Department of Transportation, Logistics and Finance, North Dakota State University
NDSU Department 2880 P.O. Box 6050, Fargo, ND 58108-6050
Phone: (701) 729-1641; Email: neeraj.dhingra@ndsu.edu; ORCiD: 0000-0002-4371-5685

*Corresponding Author

Disclosure: None.

Detecting Sources of Ride Roughness by Ensemble Connected Vehicle Signals

Abstract

It is expensive and impractical to scale existing methods of road condition monitoring for more frequent and network-wide coverage. Consequently, defects that increase ride roughness or can cause accidents will go undetected. This paper presents a method to enable network-wide, continuous monitoring by using low-cost GPS receivers and accelerometers on board regular vehicles. The technique leverages the large volume of sensor signals from multiple traversals of a road segment to enhance the signal quality by ensemble averaging. However, ensemble averaging requires position-repeatable signals which is not possible because of the low resolution and low accuracy of GPS receivers and the non-uniform sampling of accelerometers. This research overcame those challenges by integrating methods of interpolation, signal resampling, and correlation alignment. The experiments showed that the approach doubled the peak of the composite signal by decreasing signal misalignment by a factor of 67. The signal-to-noise ratio increased by 10 dBs after combining the signals from only 6 traversals. A probabilistic model developed to estimate a dynamic signal-detection threshold demonstrated that both the false-positive and false-negative rates approached zero after combining the signals from 15 traversals. The method will augment the efficiency of follow-up inspections by focusing resources to locations that consistently produce rough rides.

Keywords: Ensemble Averaging; Feature Extraction; GPS Errors; Signal Alignment; Signal-to-Noise Ratio

1 Introduction

Without frequent, network-wide condition assessments, roadway defects that increase ride roughness can go undetected and cause damages that exceed billions of dollars annually (El-Wakeel, et al., 2018). Potholes and other roadway defects that produce roughness cause many accidents (Jo & Ryu, 2015). Road roughness also adversely affects ride comfort (Cantisani & Loprencipe, 2010) and potentially human health (Múčka, 2020). Conventional approaches that use specialized vehicles and trained personnel to monitor roadways are expensive and impractical to scale across the entire network (Pierce & Weitzel, 2019). Consequently, there has been a proliferation of studies to evaluate the use of low-cost GPS receivers and accelerometers on board regular vehicles to continuously monitor the condition of roadways (Wessels & Steyn, 2020). The widespread use of smartphones equipped with all the required sensors and network connectivity have spurred many experiments. The ongoing development of standards for connected vehicles (USDOT, 2015) and the Internet-of-Things (IoT) movement has the potential for using sensors on board regular vehicles to significantly reduce the cost of network-wide and continuous condition monitoring.

The signals from low-cost accelerometers and GPS receivers in regular vehicles are likely to become available for condition monitoring applications, but their performance is not currently suitable for such high-accuracy and high-precision applications (Bridgelall, et al., 2019). Therefore, the **goal** of this research is to develop a technique that can leverage the large volume of signals available in a connected vehicle environment to enhance signal quality. The **objective** is to combine the signals from multiple traversals of a segment by ensemble averaging to reduce noise and enhance position resolution. The technique works because information signals are correlated and noise signals are uncorrelated (C.L., et al., 1975). That is, ensemble averaging will boost the information

and reduce the noise in signals, assuming that the signals are *position repeatable*. However, GPS and sampling errors create signal misalignment.

The main **contributions** of this paper are a method of signal position alignment to improve the quality of the ensemble averaging, and a method of optimally setting the signal detection threshold for the composite signal from each additional traversal to minimize both false positives and false negatives (Section 3). Section 2 discusses related work that investigated methods of processing signals from on board sensors to assess the condition of roadways. Section 4 discusses the results by quantifying the benefits of the signal alignment method. Section 5 discusses some practical considerations when applying the method. Section 6 provides some concluding remarks about the findings, prospects for generalizing the application, and comments on future work.

2 Related Works

Studies about roadway condition monitoring using connected vehicles began to gain popularity around 2014 (Bridgelall, 2014) (Dennis, et al., 2014). A recent survey of such applications revealed that the technology has matured to a point where some commercial products have become available, but many challenges remain (Salau, et al., 2019). That recent survey covered many applications of onboard sensors to monitor roadway conditions; we incorporate the survey by reference here to help keep this literature review section short.

Roadway features that causes rough rides may include speed bumps, potholes, cracks, utility covers, construction panels, debris, and rumble strips. Therefore, agencies must tag the locations of purposeful roughness features to avoid false positive detections of pavement defects. The literature also demonstrates that based on time-series data collected with smartphones, traversing rough spots such as potholes and bumps produce mainly vertical accelerations whereas vehicle acceleration and deceleration produce mainly longitudinal and rotational accelerations (Aleadelat, et al., 2018). The

vertical acceleration signals from traversing rough spots are essentially differentiated versions of the road profile that contains large peaks and valleys (Goenaga, et al., 2017).

Medina et al. (2020) found that measurements to estimate ride quality from a population of vehicles can overcome or mitigate the effects of measurement variability among different vehicles (Medina, et al., 2020). Wang et al. (2020) found that machine learning can account for variabilities in the vehicle type, speed and the type of smartphone to produce reliable predictions of vertical acceleration (Wang, et al., 2020). Except for a study that proposed several tactics to extract maximally aligned signals from a dataset without repositioning the signals (Bridgelall, et al., 2019), there have been no other demonstrations of signal quality improvement that combine the signals from multiple traversals of a road segment. Hence, there are no other work to review here.

3 Methodology

3.1 Data Collection

Given that the main purpose of this work is to demonstrate how the proposed signal alignment and ensemble averaging technique can improve signal quality to detect rough spots on a roadway more accurately, it was important that the data collection remained consistent for all traversals. Therefore, the experiments used the same vehicle (2011 Chevy Traverse), smartphone device (iPhone® 6S), and position in the vehicle (dashboard). The driver also attempted to maintain the same steady speed for each traversal. The collected data was from an experiment that the authors conducted in June 2015, using what the Minnesota Road Research Facility (MnROAD) labeled as Cell 40 at that time. There was an asphalt transitional section from Cell 40 to the adjacent cell at the time. Figure 1 shows the transition from the Cell 40 concrete panel to the asphalt section, which provided the consistent rough spot. Hence, traversing the transition produced a single isolated peak inertial event (PIE) in the signal of all traversals.

As connected vehicles were not available at the time, we emulated one by attaching a smartphone to the dashboard of a sedan. The smartphone contained all the sensors that a future connected vehicle will have to record the vertical accelerations, speed, and timestamps needed. Table 1 shows the format of the points data collected. The GPS resolution of only 3 decimal places is for illustrative purposes only. The method is independent of the type of accelerometer and GPS used, so any smartphone model would suffice for replicating the data collection when using the free PAVVET app (Lu & Bridgelall, 2016).

Figure 1. Roadway and bump traversed for the data collection.

The reference provides further details about the app and its operation. The points dataset contains geospatially tagged inertial signals from 53 traversals of a road segment that contained a single

isolated bump. The columns from left to right are time in milliseconds, vertical acceleration in g-force, instantaneous traversal speed in meters-per-second, latitude in degrees, and longitude in degrees. The pair of latitude and longitude coordinates codes the position of each GPS block as a point G_i on the map layer. Figure 2 shows the distribution of the accelerometer sampling period. The primary mode at approximately 11 milliseconds indicates that the accelerometer sampled at the rate setting most of the time, but the sample periods ranged from 1 and 18 milliseconds.

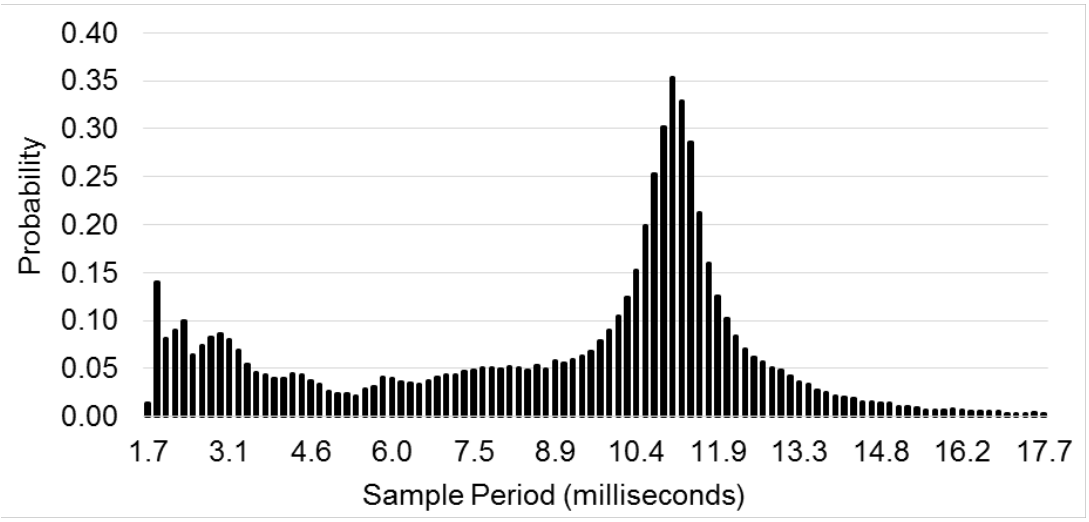

Figure 2. Sample period distribution for the inertial sensor.

The latitude and longitude remained unchanged for blocks of inertial samples because the GPS updated at approximately 1 hertz. Figure 3 graphically illustrates how the positions of the GPS updates and the accelerometer updates distribute non-uniformly both within and across traversal datasets. In the figure, N is the number of traversals and j is the traversal index. The next section describes the technique used to extract approximately equal distance traversals that are bisected by the center point.

Figure 4 plots of a small section of the first two extracted traversals, starting from the interpolated zero distance position.

Table 1. Points Data Format

Time (Seconds)	Gz (G-Force)	Speed (m s^{-1})	Lat (Degrees)	Lon (Degrees)
44.142	-1.057	9.586	45.263	-93.711
46.768	-1.216	9.586	45.263	-93.711
50.260	-1.087	9.586	45.263	-93.711
62.927	-0.854	9.586	45.263	-93.711
73.909	-0.912	9.586	45.263	-93.711
86.754	-0.942	9.586	45.263	-93.711
95.669	-1.001	9.586	45.263	-93.711
110.365	-1.022	9.586	45.263	-93.711
118.253	-1.096	9.586	45.263	-93.711
128.695	-1.013	9.586	45.263	-93.711

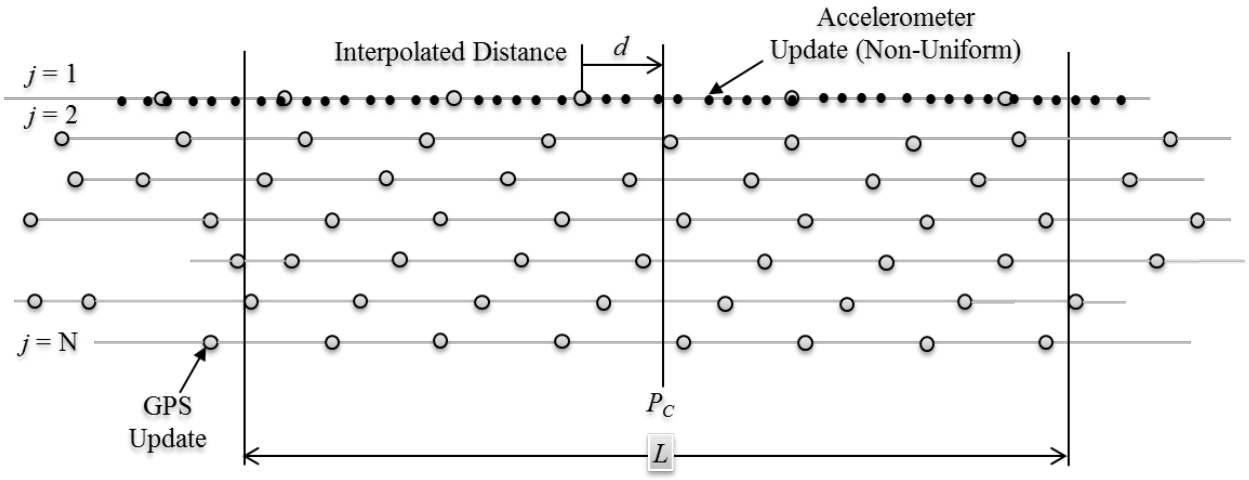

Figure 3. Spatial distribution of GPS and inertial sample updates among traversals.

The relative positions of the PIE show the amount of misalignment between the two signals. The negative peak and the positive peak of the PIE reflects the maxima and minima of the vertical acceleration profile from traversing the bump. The signals from traversing a pothole were similar but inverted.

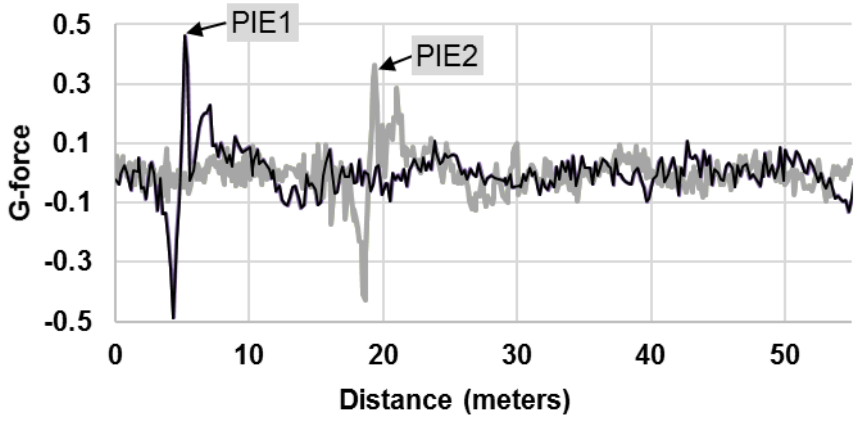

Figure 4. Position variation of the a) GPS updates b) PIE in the interpolated signal.

3.2 Problem Illustration

The effects of ensemble averaging misaligned signals are illustrated by simulating a signal using the Gaussian variant of a radial basis function (Press, et al., 2007) defined as

$$R(r) = e^{-[\epsilon(r-\rho)]^2} + \eta \quad (1)$$

where r is the distance in meters from a reference position on the traversal path, ε is the shape parameter that sets the width of the signal, ρ is the distance of the peak, and η is noise from random vibrations and electrical interference. Figure 5a simulates the position misalignment of three signals, R1 to R3, which are the elevation profiles from traversing a single isolated bump on a smooth surface. Figure 5b shows the ensemble average of the position misaligned signals relative to the position aligned signals. The simulation of a bump is a generalization of a rough spot that produces signal peaks and valleys. For instance, the inverse of a bump would simulate a simple pothole—inverses of the signals in Figure 5a. That is, multiplying the radial basis function by -1 achieves the simulation of a pothole. Hence, the signal detector identifies either negative or positive peaks as rough spots. Taking the absolute value of the signal simplifies the peak detection by using only

positive thresholds. Ensemble averaging reduced the noise by a factor of two for either the aligned or non-aligned signals.

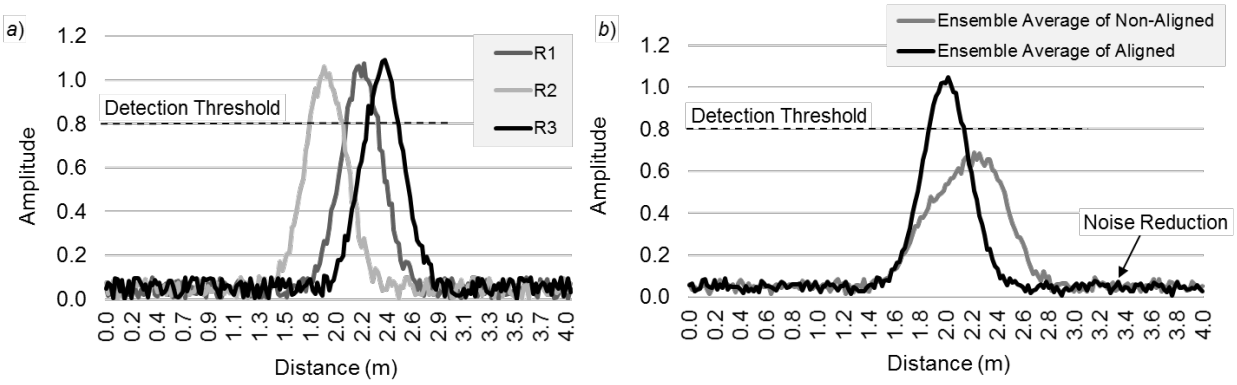

Figure 5. Simulation of a) individual signals and b) their ensemble averages.

However, a misalignment spread of 0.7 meters for a one-meter-wide bump signal decreased the peak of the composite signal by one-third, biased the peak by 0.4 meters, and nearly doubled the width. Hence, these adverse effects decreased both the accuracy and precision of estimating the position of a rough spot that produced the signal. At a hypothetical signal detection threshold of 0.8, signal misalignment would have caused a false negative for the composite signal. Section 3.8 discusses a method for selecting the best threshold.

Position misalignment is due to the following:

1. Accelerometer non-uniform sample period and spatially asynchronous updates (Bridgelall, 2014).
2. GPS receiver low accuracy, low precision, and spatially asynchronous updates (Bajaj, et al., 2002).

Figure 2 illustrates the first source of misalignment, which was the accelerometer sample period variation. The non-uniform sampling caused each signal to have a different number of samples, and the distances associated with each sample was also non-uniformly distributed. Even with uniform

sampling, the distances associated with each sample will be misaligned because of the asynchronous spatial updates among traversals.

GPS, the second source of misalignment, has the following five characteristics:

1. Standard low-cost GPS receivers provide position updates each second (Hunter, et al., 2009). Hence, GPS coordinates will update after groups of 64 inertial samples when using an inertial sensor that samples at 64 hertz. Therefore, blocks of 64 samples will have the same GPS coordinate tags. These *GPS blocks* lower position resolution lacks information for signal alignment.
2. Position updates among traversals are not repeatable in space. That is, each traversal will have different geospatial coordinates along the path, and some updates will miss signal peaks.
3. Some position updates will deviate from the travel path because of two-dimensional position errors.
4. The GPS position error along the traversal path is three to five meters (Hughes, 2016).
5. Clouds, trees, or tunnels could block the reception of GPS signals in some locations (Groves, et al., 2012).

Figure 6 illustrates the second, third, and fourth sources of misalignment from GPS issues. The figure plots the geospatial position updates for the first two traversals taken from the dataset used in this study. The square and star symbols are the GPS updates from Traversal 1 and Traversal 2, respectively. The geospatial updates for each traversal appear uniform. However, the updates between the two traversals are spatially asynchronous because they occur in different locations and time, which illustrates the *second* issue. It is also evident that the geospatial position updates of Traversal 2 are mostly off the traversal path, which illustrates the *third* issue. The small cluster of

points shown in Figure 6 that falls to the right of the reference line R0 are the geospatial positions of the GPS blocks containing the PIE from each traversal. Although the bump did not move, the position spread of the PIE in the signal was 30.4 meters along the traversal path and 14.5 meters perpendicular to the traversal path, which illustrates the *fourth* issue. Hence, the variations in the relative distances of the PIE in this dataset characterizes the amount of signal misalignment that would be expected.

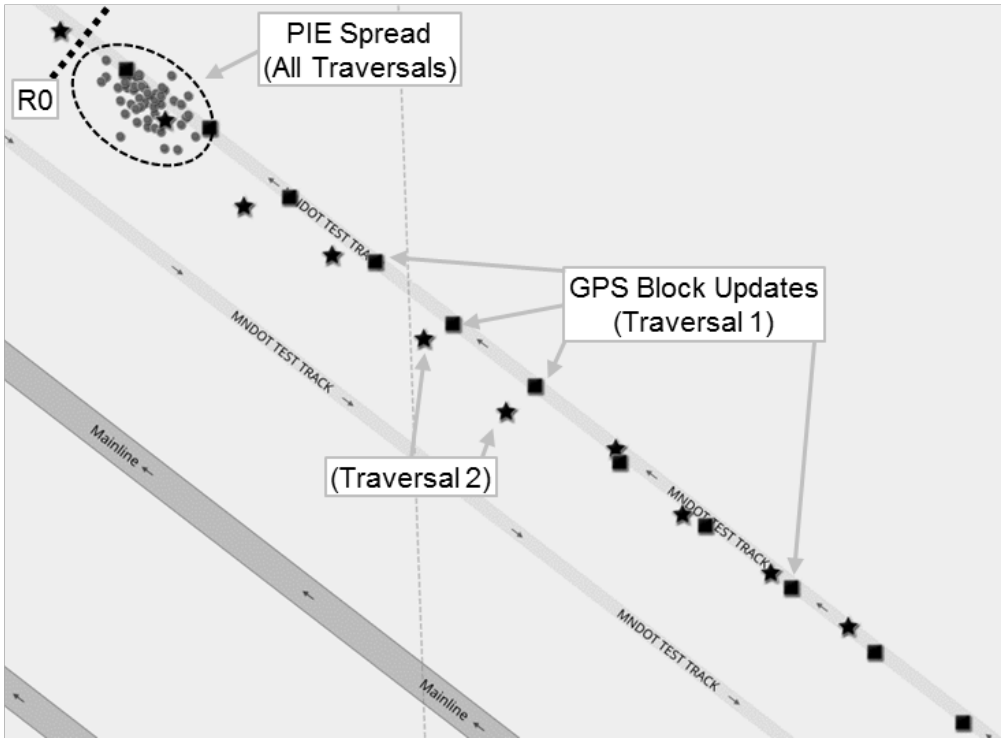

Figure 6. Geospatial position variation of the GPS updates among traversals.

3.3 Signal Processing Workflow

The signal processing workflow begins by using a geographic information system (GIS) to identify, from a map, the road segments for analysis. Figure 7 shows the procedures of the signal processing workflow. The *first* procedure uses GIS to create a network layer with points P_c that mark the center of each segment that has associated data. Each point of the segment layer must also contain an

attribute L to specify the length of the marked segment. The *second* procedure uses a GIS technique that spatially joins the points layer of traversal data to the marked segment layer. The *third* procedure extracts data representing approximately equal length traversals on either side of point P_c. The *fourth* procedure resamples the accelerometer signals with uniform distance spacings, which prepares the signals for the *fifth* procedure of correlation alignment. The *sixth* and final procedure ensemble averages the position aligned signals to achieve enhanced SNR. The signal processing workflow does not show the final application of setting an optimum signal detection threshold to minimize both false positives and false negatives.

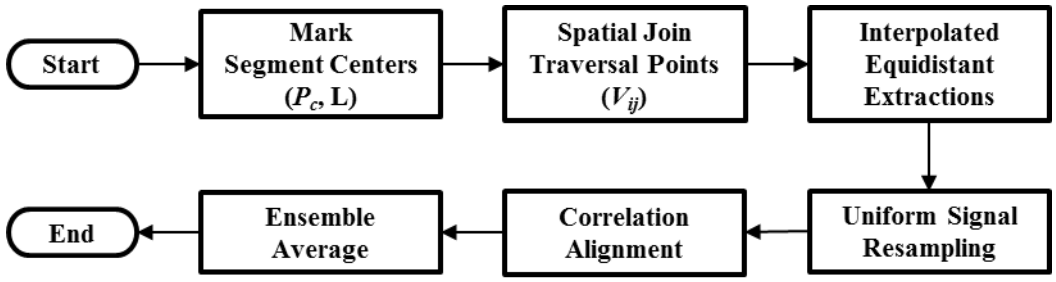

Figure 7. Signal processing workflow for ensemble signal combination.

The next subsections describe the algorithms for each of the procedures in the signal processing workflow.

3.4 Interpolated Equidistant Extraction

Distance interpolation is needed to tag the inertial signal samples with higher-precision distances because GPS provides only a course update of distance from the center point P_c. The interpolation uses the speed and sample intervals in the dataset to accumulate distances from a reference point. The distance for the first reference point x_0 is set to zero, and the distance x_n for subsequent samples are

$$x_n = x_{n-1} + v_n \times \Delta\tau_n \quad (2)$$

where n is the sample number, v_n is the instantaneous speed for sample n, and $\Delta\tau_n$ is associated with the sample period. The distance precision is dictated by the accelerometer sample period, which is several orders of magnitude smaller than the GPS update interval.

Figure 8 displays the algorithm for interpolated equidistant extractions. The algorithm is applied to every traversal in the data set. The algorithm first finds the GPS block that is closest to the left of point P_c and then distance interpolates the accelerometer samples to the right until the distance is closest to the position of P_c. This marks the starting index for leftward interpolation to reach an approximate distance equal to $L/2$, which would be the first sample g_0 for the extracted traversal. Finally, interpolating distance rightward to approximately L yields the last sample g_L for the extracted traversal. Alternatively, interpolating left and then right from the sample closest to P_c to approximately $L/2$ would be more efficient, but that would require an additional step to relabel positive and negative distances to positive only distances, starting with distance zero. The proposed approach is compatible with traditional linear referencing techniques that specify distances from a reference position such as a milepost or a landmark to improve accuracy and practicality in fieldwork (Curtin, et al., 2007). In this case, the geospatial reference position for distance zero will be the coordinates of a point located at the path distance of L/2, to the left of P_c. The operator $\|P_c - G_i\|$ shown in the algorithm produces the geodesic distance between two perpendicular lines that bisect the geospatial points P_c and G_i. The $\min_{\text{Left}}\{\}$ function is a GIS procedure that finds the GPS point i that is closest to the left of P_c.

Interpolated Equidistant Extraction

Inputs:
  L # Length of segment
  Pc # Coordinates of a point at the center of the segment
  V # Points table [speed, sample time, GPS coordinates]
Begin:
  $V_c \leftarrow \min_{Left}\{\|P_c - V\{G_i\}\|, \forall i\}$ # Get the GPS block Vc closest to the left of Pc
  $V_c\{x_0\} \leftarrow 0$ # Add distance column with first sample distance = 0
  do
    $V_c\{x_{k+1}\} \leftarrow V_c\{x_k\} + V_c\{v_{k+1}\} \times V_c\{\Delta\tau_{k+1}\}$ # Interpolate next distance
    $k \leftarrow k + 1$ # Increment table index to the right
  until $\min_k\{\|P_c - V_c\{G\}\| - V_c\{x_k\}\}$ # Stop after finding sample closest to Pc
  $V_c\{x_k\} \leftarrow 0$ # Initialize as starting sample for left interpolation
  do
    $V\{x_{k+1}\} \leftarrow V\{x_k\} + V\{v_{k+1}\} \times V\{\Delta\tau_{k+1}\}$ # Interpolate distance (entire table)
    $k \leftarrow k - 1$ # Decrement table index to the left
  until $\min\left(\frac{L}{2} - V\{x_k\}\right)$ # Stop after distance is closest to L/2
  $g_0 \leftarrow k$ # Store first index of the extracted traversal
  $V\{x_k\} \leftarrow 0$ # Initialize starting distance
  do
    $V\{x_{k+1}\} \leftarrow V\{x_k\} + V\{v_{k+1}\} \times V\{\Delta\tau_{k+1}\}$ # Interpolate next distance
    $k \leftarrow k + 1$ # Increment table index to the right
  until $\min(L - V\{x_k\})$ # Stop after distance is closest to L
  $g_L \leftarrow k$ # Store last index of the extracted traversal
End:
Outputs: g_0, g_L # Start and end table indices (extracted traversal)

Figure 8. Traversal extraction algorithm with linear referencing.

3.5 Uniform Signal Resample

The distance interpolated traversals have approximately equal distances. However, the number of samples vary because of non-uniform sampling. The cross-correlation approach requires that all signals have the same number of samples and represent the same distance positions. The solution was to resample all the signals at the same uniformly spaced distances by using a signal interpolation technique. Figure 9 displays the uniform signal resample algorithm. The inputs S_M and D_M are the numbers of samples and distance of a reference signal in the dataset. The reference signal is selected as the signal with the most samples because it represents the highest distance precision available in the dataset. For each traversal, the uniform signal resample algorithm first defines the function $f(\boldsymbol{x})$ based on the original distance vector $\boldsymbol{x}$ and the signal vector $\boldsymbol{y}$. The algorithm next creates a new

vector $\hat{\boldsymbol{x}}$ that has the same number of samples and distances as the reference signal. Using the defined function *f*, the algorithm then estimates a new signal by evaluating the function at the new uniformly spaced distances in vector $\hat{\boldsymbol{x}}$. Several signal interpolation techniques can be used to estimate the values of the function at new distance positions. One of the simplest is linear interpolation. Given samples y_i and x_i, linear interpolation produces a new sample $\hat{y}$ within the interval (y_i, y_{i+1}) that is associated with a value of x within the interval (x_i, x_{i+1}) such that

$$\hat{y} = \frac{y_{i+1} - y_i}{x_{i+1} - x_i}(x - x_i) + y_i \tag{3}$$

With all extracted traversals resampled at identical and uniformly spaced distances, they are now ready for correlation alignment.

Uniform Signal Resample

Inputs:
- $\mathbb{T}$ # Extracted traversal tables [signal, distance]
- SM # Number of samples (rows) of reference signal.
- DM # Distance of reference signal.

Begin:

For $\forall j \in \mathbb{T}$

- $y_{ij} = f(x_{ij})$ # Define y(x) at the original distances
- $\hat{x}_{ij} = i\frac{D_M}{S_M}, i = \{0,1, \ldots (S_M - 1)\}$ # Create new uniformly sampled distances
- $\hat{y}_{ij} = f(\hat{x}_{ij})$ # Estimate y(x) at new distances

End:

Outputs:
- $\mathbb{T}$ # Uniformly resampled traversals (Signal, Distance)
- R # Index of the reference signal in the dataset

Figure 9. Traversal interpolation algorithm.

3.6 Correlation Alignment

The inputs to the correlation alignment algorithm, shown in Figure 10, are the tables of uniformly resampled signals, the reference signal identified by its index *R*, and the number of samples S_M in the reference signal. The algorithm performs a cross-correlation between the reference signal and the signals of all the other traversals. The shift position of maximum cross-correlation is determined by the function $\max_{\forall k}(r_k)$. It is possible that there will be more than one value that is equal to the

maximum value in the cross-correlation vector r_k. Therefore, the operator $\langle\cdot\rangle$ is used to return the index of the first maximum value. The shift position is relative to the distance of the first sample of the reference signal, which is zero. Hence, the position of zero shift is when the distance labels of both vectors overlap. This is the default shift position when there are no signals to correlate, which means that all the sensor samples contain only noise. Negative and positive shift values represent shifts to the left and right of the overlapping position, respectively. The shifted signal inherits the distance labels of the reference signal. When the shift is positive, the first sample of the shifted signal will inherit the distance labels starting at the shifted number of positions to the right of the distance vector of the reference signal.

Correlation Alignment

Inputs:
- $\mathbb{T}$ # Uniformly resampled signal tables [signal, distance]
- R # Index of reference signal
- S_M # Number of samples in the reference signal.

Begin:

For $\forall j \in \mathbb{T}$

$r_{kj} = \sum_{n=0}^{S_M-1} \hat{x}_{n,j} \times \hat{x}_{n-k+S_M-1,R}\,,\ k = \{0,1,\dots(2S_M-2)\}$ # Cross-correlate

$s_j \leftarrow \langle \max_{\forall k}(r_{kj}) \rangle - S_M + 1$ # Shift position of maximum cross-correlation

If $s_j > 0$ # Positive shift

$x_{ij} = \hat{x}_{ij},\ \ i = \{s_j, s_j+1, \dots(S_M-1)\}$ # Advance distance vector

$y_{ij} = \hat{y}_{ij},\ \ i = \{0,1,\dots(S_M-1-s_j)\}$ # Truncate signal vector

Else

$x_{ij} = \hat{x}_{ij},\ \ i = \{0,1,\dots(S_M-1-|s_j|)\}$ # Truncate distance vector

$y_{ij} = \hat{y}_{ij},\ \ i = \{|s_j|, |s_j|+1,\dots(S_M-1)\}$ # Advance signal vector

End:

Outputs: $\mathbb{T}$ # Aligned signal tables [signal, distance]

Figure 10. Correlation alignment algorithm.

This is equivalent to advancing the distance vector of the signal by the number of shift positions for maximum cross-correlation. The tail will be ahead of the last sample of the reference signal because the signal is advanced, and is, therefore, truncated. The reverse procedure is used when the shift position for maximum cross-correlation is negative.

3.7 Ensemble Average

The realignment of signals resulted in a variation of the distance positions for the first and last samples across the aligned traversal dataset. Hence, prior to ensemble averaging, the algorithm trims the aligned signals so that the beginning and ending positions are equal to the maximum and minimum values, respectively. Finally, the ensemble average of the signal at position k is the mean value of the signal across all traversals, at that position. Figure 11 shows the ensemble averaging algorithm.

Ensemble Average

Inputs:
  $\mathbb{T}$ # Tables of aligned signals [signal, distance]
  SM # Number of samples
Begin:
  For $\forall j \in \mathbb{T}$
    $L_{\max} \leftarrow \max_{\forall j \in \mathbb{T}} x_{0,j}$ # Maximum of starting distances
    $R_{\min} \leftarrow \min_{\forall j \in \mathbb{T}} x_{S_M - 1,j}$ # Minimum of ending distances
    $x_{Lj} \leftarrow \min_{\forall k} \left| x_{kj} - L_{\max} \right|, x_{Rj} \leftarrow \min_{\forall k} \left| x_{kj} - R_{\max} \right|$ # First and last samples
  $Y_k = \frac{1}{T} \sum_{j=0}^{T-1} y_{kj}\ ,\ k = \{0,1, \dots\}$ # Ensemble average signal across position k
End:
Outputs: W # Vector [ensemble averaged signal, distance]

Figure 11. Ensemble averaging algorithm.

3.8 Detection Threshold Model

In signal detection theory, a *false positive* or *type I* error means that the detector falsely reported a noise event as an inertial event. A *false negative* or *type II* error means that the detector failed to identify a true inertial event in the signal. Setting the optimum signal detection threshold for a given SNR involves a tradeoff that minimizes both types of errors (Chen, 2004). Setting the threshold too low will increase false positives because noise will trigger a detection. Increasing the threshold will decrease false positives but setting the threshold too high will increase false negatives because the detector could miss signals.

Figure 5b shows that the ensemble average of aligned signals produces a clearly isolated signal peak, whereas signal misalignment lowers the signal level and broadens the peak. Hence, signal misalignment forces a lowering of the signal detection threshold to prevent a false negative, which also increases the probability of a false positive from noise peaks. As shown, in both cases ensemble averaging decreases the noise, which increases the SNR asymptotically with each additional signal combined. A larger SNR increases the gap between signals and noise so that the optimum signal detection threshold would further minimize both type I and type II errors. Hence, a model is needed to inform the optimum signal detection threshold for the composite signal as a function of the number of traversals combined.

From statistics, if P_1 is the probability of detecting the signal, then the probability of not detecting the signal is $(1 - P_1)$. Hence, the probability of still not detecting the signal after n consecutive traversals is $(1 - P_1)^n$ so long as the detection attempts are independent. Therefore, the probability of detecting the signal after n consecutive traversals is

$$P(n) = 1 - (1 - P_1)^n \tag{4}$$

with a boundary condition check that when $n = 1$ the function evaluates to $P(1) = P_1$. Figure 12a plots the function $P(n)$ for various values of P_1 and n. This n-trial probability asymptotically approaches 100% and the rate of approach is faster as P_1 increases.

The probability P_1 of detecting the signal as a function of a signal detection threshold x can be determined from the dataset by estimating a probability density function $f(x)$ from a histogram of the signal peaks. Then the cumulative probability $F(x)$ of detecting signal levels below x is

$$F(x) = \int_0^x p(x)\, dx \tag{5}$$

Finally, the reverse cumulative probability function $R(x) = 1 - F(x)$ relates the signal detection threshold x to the probability of signal detection P_1 where

$$x = R^{-1}(P_1). \tag{6}$$

Figure 12b illustrates the probability of signal detection P_1 as a function of the signal detection threshold x for a Gaussian distribution of peak signal values. For illustration, the simulation uses a mean signal peak value of 0.5 g and a standard deviation of 0.1 g. Hence, setting a signal detection threshold at 0.4, for example, will result in detecting the signal in the first attempt with a probability of 80%. Lowering the threshold towards zero increases P_1 towards 100%. However, unless noise is reduced, lowering the threshold will also increase false positives by erroneously detecting noise peaks as signals. Ensemble averaging reduces noise asymptotically towards zero as the signal level approaches the mean value. Therefore, the SNR will increase asymptotically.

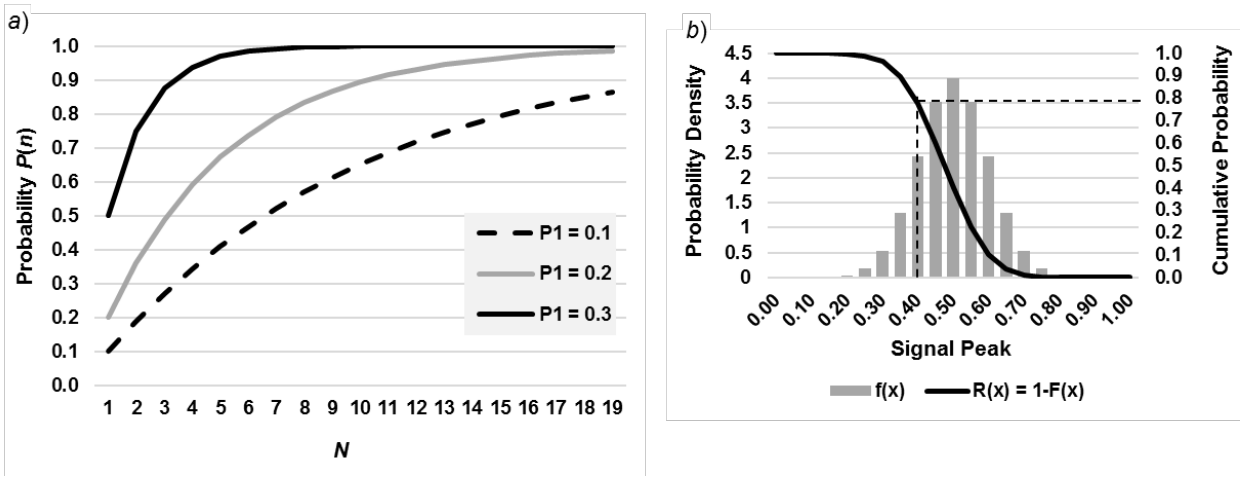

Figure 12. Probability of detection a) after n trials and b) as a function of threshold level.

It is natural to estimate the n-trial probability from measurements of the SNR because both functions increase asymptotically with the inclusion of additional signals into the ensemble average. The association is a direct proportionality such that

$$SNR(n) = \alpha[1 - (1 - P_1)^n] \quad (7)$$

where α and P_1 are constants that can be estimated from the data. The initial signal detection threshold will be the value associated with the estimate of P_1 as determined from a histogram of the signal peaks. Subsequently, the technique to evaluate the potential type I and type II error rates as a function of the number of traversals combined uses the following procedure:

1. After signal alignment, compute the SNR from an ensemble average of n signals.
2. Fit the n-trial probability function to the SNR data to estimate P_1 .
3. Plot a reverse cumulative histogram of the signal peak to identify the initial signal detection threshold x_1 associated with P_1.
4. Record the factor $\gamma = x_1/\rho_1$ where ρ_1 is the root-mean-squared value of the noise level of the first signal.
5. Determine the minimum number of traversals N needed for P_N to approach 1, which represents a false negative rate approaching zero.
6. Determine the new noise level ρ_N of the composite signal combining N traversals.
7. Determine the associated signal detection threshold level as $x_N = \gamma\, \rho_N$.

This procedure reduces the signal detection threshold by the same amount as the noise reduction achieved with each additional signal included in the ensemble average. Hence, the procedure lowers the signal detection threshold while keeping it above the new noise level by the same factor γ. The result is a consistent lowering of the signal detection threshold towards the minimum signal value to approach zero false-negative without changing the false positive rate.

4 Results

Signal position alignment and ensemble averaging boosted the signal and decreased the noise by reducing the positional variation of the signal. Table 2 compares the means (μ) and standard

deviations (σ) of the distance differences between the PIE of each signal and that of the reference signal, denoted as ΔPIE.

Table 2. Evaluation of the Signal Alignment Method

	ΔPIE (m)		EA Peak
Description	μ	σ	(g)
Non-aligned signals	0.57	6.07	0.46
Aligned signals	0.11	0.09	0.99
Improvement Factor	5.1	67.4	2.14

After applying the *centroid truncate* method prior to alignment, the spread of ΔPIE was more than 6 meters. The subsequent application of *correlation alignment* decreased the mean and the spread of ΔPIE by a factor of more than 5 and 67, respectively. The improvement in alignment boosted the peak of the ensemble averaged (EA) signals by a factor of more than two, which is approximately 3 dBs of signal gain.

Figure 13 plots the SNR of the ensemble-averaged signals as a function of the number of traversals combined. In engineering, it is customary to report SNR measurements in decibel (dB) units where increasing values indicate improvement. The results show that ensemble averaging increased the SNR by 9.8 dB after combining the signals from the first 6 traversals. With perfect alignment, the SNR will increase continuously. However, because the alignment is not perfect, random variations in the relative position of the signal peaks cause a jagged SNR trend in the composite signal, albeit with the overall trend increasing asymptotically to a maximum value. Fitting the *n*-trial probability function to the SNR data provided an estimate of 0.51 for P_t. Table 3a summarizes the parameter estimates, and Table 3b lists the SNR data and values evaluated for the best fit. The coefficient of determination R^2 of 0.90 suggests that the fit is very good.

For this dataset, a reverse cumulative histogram of the signal peaks established that a signal detection threshold associated with $P_t = 0.51$ would be $\gamma = 4.4$ times above the noise level.

Table 3. a) Parameters of Best-fit Function and b) the SNR Data

a) Function Parameters		
R2	Pt	α
0.90	0.51	23.25

b) SNR Data and Fit		
N	Data (dB)	Fit (dB)
1	14.31	11.84
2	16.83	17.66
3	18.99	20.51
4	20.87	21.91
5	21.74	22.59
6	24.13	22.93
7	22.77	23.10
8	22.85	23.18
9	23.19	23.22
10	24.51	23.24
11	23.44	23.25
12	23.39	23.25
13	23.66	23.25
14	23.21	23.25
15	23.11	23.25

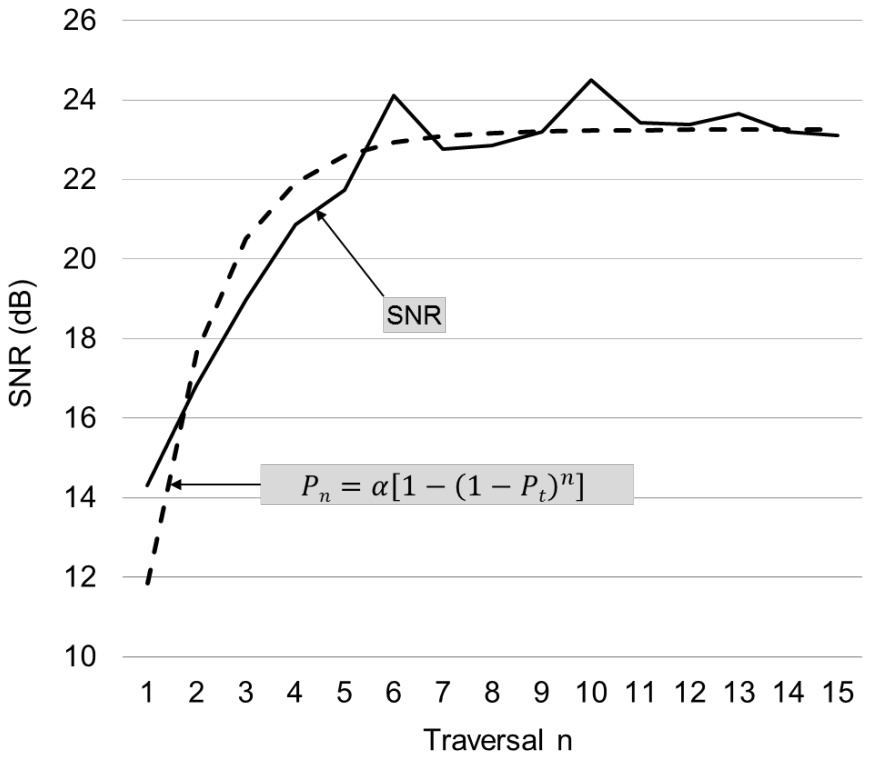

Figure 13. SNR and fitted n-trial probability function.

At that level, there were no false positives in the dataset. However, the false negative rate at signal detection threshold x_1 was $[1 - P_t] = 0.49$ for individual signal detections. For the dataset, there were no false negatives for the threshold x_6. This required maintaining the signal detection threshold at $\gamma = 4.4$ times above each of the new noise levels ρ_n after ensemble averaging. As shown in Figure 13, the fitted probability curve suggests that with $\alpha = 1$, the false-negative rate will approach zero after combining the signals from 15 traversals.

5 Discussion

To apply the method in practice, a method of *linear referencing* is needed to identify the zero-distance position. Many textbooks on geographic information systems (GIS) include an in-depth discussion on methods of linear referencing (Curtin, et al., 2007). In its simplest form, the geospatial position associated with a landmark or a milepost is most often used in transportation-related fieldwork. When applying the method developed in this paper, the reference position would be a geospatial coordinate associated with the first GPS block of the aligned signals. However, given the large variation in GPS positions, a method is needed to identify a single geospatial position. The recommended approach is to use the common “snap” feature of most GIS tools to move the points of all GPS blocks onto the centerline of the path, and then to compute the centroid of the resulting points from the first adjusted GPS block of the aligned signals. The centroid is a good statistical estimator for the spatial position of the zero-distance position along the traversal path. Subsequently, a follow-up inspection will locate the rough spot by following any lane of the curvilinear path, from the reference centroid location to the specified offset distance. The rough spot could be on any lane of the curvilinear path but still within line-of-sight of an inspector.

Another consideration is that, because the ensemble averaging required truncating the signals to approximately equal length after realignment, the segments to be analyzed should be overlapped

by at least the measured spread of the first GPS block. This will avoid the potential miss of a rough spot at the segment fringes due to signal truncation.

The proposed method estimated the best signal detection threshold based on the data that was collected. The best signal detection threshold depends on the level of signal alignment achieved. That is, the signal detection threshold depends on the SNR trend, which provides an estimate for the probability of detecting a signal after a single attempt. The accuracy of signal alignment is affected by variations in the signal levels, GPS update rate, and accelerometer update rate among traversals. Hence, a repeat of the procedures in the proposed method is recommended for any new data collected with different sensors, placement of sensors, vehicles used, and traversal speeds.

Yang et al. (2020) recently addressed issues relating to the need for sensor calibration to account for sensor and vehicle variations (Yang, et al., 2020). That is, the signal level depends on the dampening effects of the sensor, the vehicle suspension system, and the vehicle speed. Hence, Bridgelall et al. (2019) addressed issues related to non-uniform vehicle speeds (Bridgelall, et al., 2019). This work focused on enhancing the signal-to-noise ratio through ensemble averaging of aligned signals, regardless of such anticipated variations in the signal measurement conditions. To avoid averaging low signal levels due to exceptionally low speed traversals or excessive suspension system dampening, the workflow removed traversals without absolute value signal peaks that are twice the average noise level. Although obvious, it is important to note that the method detects rough spots only on paths that vehicles traverse.

6 Conclusion

The ubiquitous connectivity of vehicles can enable frequent and network-wide monitoring of infrastructure condition by using on board sensors to measure and report roughness levels. However, the application of signal detection techniques to sensor data from a single traversal can lead to high

false-positive and high false-negative rates. Ensemble averaging the signals from multiple traversals can reduce noise and, therefore, reduce the false-positive rate for a given signal detection threshold. However, signal position misalignment from variations in the accelerometer update rate, GPS position errors, and low distance resolution degrades the quality of the composite signal. This work developed a technique that uses distance interpolation, signal resampling, and cross-correlation to align the position of all signals of the dataset.

The correlation alignment method decreased the mean deviation and spread from a reference signal by a factor of more than 5 and 67, respectively. The signal peak from ensemble averaging all the aligned signals of the dataset was double that of the result from ensemble averaging the non-aligned signals. Adding aligned signals to the ensemble averaging resulted in a 10 dB increase in SNR after combining the first 6 signals. An *n*-trial probability model fitted to the data informed the optimum threshold for signal detection as a function of the number of traversal signals combined. The result was that both the false positive and false negative rates approached zero after combining the signals from the first 15 traversals. The model suggests that the signal quality will improve continuously as more data becomes available. Hence, the method of correlation alignment with ensemble averaging can be generalized for applications that produce geospatial sensor data from multiple observations of a phenomenon.

Future work will extract features from the composite signals to develop machine learning models that can be trained to classify the types of rough spots detected. This capability will inform preparations for a follow-up inspection to select the appropriate tools and equipment that can further validate the presence of that type of issue.

7 Data Availability Statement

Some or all data, models, or code that support the findings of this study are available from the corresponding author upon reasonable request. The data collected with the PAVVET app is in CSV format.

8 Acknowledgment

Funds from the North Dakota State University and the Mountain-Plains Consortium, a University Transportation Center funded by the U.S. Department of Transportation supported this work. The contents of this paper reflect the views of the authors, who are responsible for the facts and accuracy of the information presented.

9 References

Aleadelat, W., Ksaibati, K., Wright, C. H. G. & Saha, P., 2018. Evaluation of Pavement Roughness Using an Android-Based Smartphone. *Journal of Transportation Engineering, Part B: Pavements,* 144(3), p. 4018033.

Bajaj, R., Ranaweera, S. L. & Agrawal, D. P., 2002. GPS: location-tracking technology. *Computer,* 35(4), pp. 92-94.

Bridgelall, R., 2014. Connected Vehicle Approach for Pavement Roughness Evaluation. *Journal of Infrastructure Systems,* 23 April, 20(1), pp. 04013001 (1-6).

Bridgelall, R., 2014. Inertial Sensor Sample Rate Selection for Ride Quality Measures. *Journal of Infrastructure Systems,* 21(2), pp. 04014039 (1-5).

Bridgelall, R. et al., 2019. Enhancement of signals from connected vehicles to detect roadway and railway anomalies. *Measurement Science and Technology.*

Bridgelall, R., Hough, J. & Tolliver, D., 2019. Characterising pavement roughness at non-uniform speeds using connected vehicles. *International Journal of Pavement Engineering,* 20(8), pp. 958-964.

C.L., W. et al., 1975. Ensemble Averaging of Repeatable Noisy Signals. In: *Digital Electronics and Laboratory Computer Experiments.* Boston(MA): Springer.

Cantisani, G. & Loprencipe, G., 2010. Road Roughness and Whole Body Vibration: Evaluation Tools and Comfort Limits. *Journal of Transportation Engineering-asce,* 136(9), pp. 818-826.

Chen, C.-T., 2004. *Signals and Systems.* 3rd ed. New York: Oxford University Press.

Curtin, K. M., Nicoara, G. & Arifin, R. R., 2007. A comprehensive process for linear referencing. *URISA Journal,* 19(2), pp. 41-50.

Dennis, E. P. et al., 2014. Pavement condition monitoring with crowdsourced connected vehicle data. *Transportation Research Record,* 2460(1), pp. 31-38.

El-Wakeel, A. S. et al., 2018. Towards a practical crowdsensing system for road surface conditions monitoring. *IEEE Internet of Things Journal,* 5(6), pp. 4672-4685.

Goenaga, B. J., Pumarejo, L. G. F. & Lerma, O. A. M., 2017. Evaluation of the methodologies used to generate random pavement profiles based on the power spectral density: An approach based on the International Roughness Index. *Revista Ingenieria E Investigacion,* 37(1), pp. 49-57.

Groves, P. D., Wang, L. & Ziebart, M., 2012. Shadow Matching: Improved GNSS Accuracy in Urban Canyons. *GPS World,* 23(2), pp. 14-18.

Hughes, W. J., 2016. *Global Positioning System (GPS) Standard Positioning Service (SPS) Performance Analysis Report,* Washington, D.C.: Technical Center.

Hunter, T., Herring, R., Abbeel, P. & Bayen, A., 2009. *Path and travel time inference from GPS probe vehicle data.* Vancouver, Canada, Neural Information Processing Systems (NIPS) Foundation, pp. 1-8.

Jo, Y. & Ryu, S., 2015. Pothole detection system using a black-box camera. *Sensors,* 15(11), pp. 29316-29331..

Lu, P. & Bridgelall, R., 2016. *An Intelligent Transportation Systems Approach to Railroad Infrastructure Performance Evaluation: Track Surface Abnormality Identification with Smartphone-Based App,* Fargo, ND: Mountain-Plains Consortium.

Medina, J. R., Ramadan Salim, B. S. U. & Kaloush, K., 2020. Experimental Study for Crowdsourced Ride Quality Index Estimation Using Smartphones. *Journal of Transportation Engineering, Part B: Pavements,* 146(4), p. 04020070.

Múčka, P., 2020. Vibration Dose Value in Passenger Car and Road Roughness. *Journal of Transportation Engineering, Part B: Pavements,* 146(4), p. 4020064.

Pierce, L. M. & Weitzel, N. D., 2019. *NCHRP Synthesis 531: Automated Pavement Condition Surveys,* Washington, D.C.: National Cooperative Highway Research Program (NCHRP).

Press, W. H., Teukolsky, S. A., Vetterling, W. T. & Flannery, B. P., 2007. *Numerical Recipes 3rd Edition: The Art of Scientific Computing.* s.l.:Cambridge University Press.

Salau, H. B. et al., 2019. A Survey of Accelerometer-Based Techniques for Road Anomalies Detection and Characterization. *International Journal of Engineering Science and Application,* 3(1), pp. 8-20.

USDOT, 2015. *Beyond Traffic 2045: Trends and Choices.* Washington, D.C.: United States Department of Transportation.

Wang, G., Burrow, M. & Ghataora, G., 2020. Study of the Factors Affecting Road Roughness Measurement Using Smartphones. *Journal of Infrastructure Systems,* 26(3), p. 04020020.

Wessels, I. & Steyn, W. J. V. d. M., 2020. Continuous, response-based road roughness measurements utilising data harvested from telematics device sensors. *International Journal of Pavement Engineering,* 21(4), pp. 437-446.

Yang, X. et al., 2020. Calibration of smartphone sensors to evaluate the ride quality of paved and unpaved roads. *International Journal of Pavement Engineering,* pp. 1-11.